Dalton Transactions

Accepted Manuscript

ROYAL SOCIETY OF CHEMISTRY

www.rsc.org/dalton

Journal Name

ARTICLE TYPE

Cite this: DOI: 10.1039/xxxxxxxxxx

Microporous Aluminophosphates Synthesized with 1,2,3-Trimethylimidazolium and Fluoride†

Jeong Hwan Lee,[a] Eun Jeong Kim,[a] Fernando López-Arbeloa,[b] Suk Bong Hong*[a] and Miguel A. Camblor*[c]

Received Date
Accepted Date

DOI: 10.1039/xxxxxxxxxx

www.rsc.org/journalname

The synthesis of microporous aluminophosphates using 1,2,3–trimethylimidazolium (123TMI) and fluoride produces three phases (HPM–3, PST–27 and triclinic $AlPO_4$–34) depending on the amount of water and organic structure-directing agent in the synthesis mixture. Fluoride occluded in double 4-ring units was not detected by ^{19}F MAS NMR spectroscopy in any product. While the structure of HPM–3 remains unknown, PST–27 has been determined to be a monoclinic version of $AlPO_4$–5 with a distorted and likely complex structure. Rietveld analysis using synchrotron diffraction data for as-made triclinic $AlPO_4$–34 reveals that each of its *cha*–cages holds two 123TMI cations, forming a displaced anti-parallel dimer with a short distance between aromatic rings (3.78 Å from center to center, 3.63 Å from plane to plane). This suggests that $\pi-\pi$ interactions may play a role in the synthesis of this phase and related CHA-type systems. A study of the optical properties of PST–27, $AlPO_4$–34 and other materials containing 123TMI cations shows their complex fluorescence behavior, sometimes displaying a red-edge effect, i.e., a red shift of the fluorescence as the excitation wavelength is shifted toward the red edge of the absorption band. An absorption band at 291 nm appears only in the dimer–containing triclinic $AlPO_4$–34 and is sensitive to the introduction of Si in the framework.

1 Introduction

Crystalline microporous aluminophosphates ($AlPO_4$'s), and their metalloaluminophosphate (MeAPO) and silicoaluminophosphate (SAPO) counterparts, constitute a class of zeolite-like materials with potential for certain applications.[1] One of the important characteristics of $AlPO_4$ framework materials is the strict alternation of Al and P, implying that the structures can only contain rings with an even number of tetrahedra, which is also true for the MeAPO and SAPO versions.

We have previously studied the structure direction of imidazolium cations and fluoride anions in the silica[2,3–9] and aluminosilicate systems.[10] While fluoride tends to yield structures containing double-four membered rings (D4R),[3,7,11–16] the imidazolium cations we have tried so far can yield a number of zeolites with (Zeolite Framework Types ITW, STW)[17] or without D4R (MTW, TON, MFI, RTH). All of them, however, also contain 5-membered ring (5MR) units. The study of the performance of imidazolium cations as organic structure-directing agent (OSDA) in the $AlPO_4$ system may in our opinion be merited, because large differences are anticipated: since 5MR are considered impossible in the fully connected $AlPO_4$ system because of the need to alternate Al and P, the known structure–direction exerted by imidazolium cations would be frustrated in the $AlPO_4$ system, and hence structures different form those observed in the silica-based system should be obtained. In addition to these topological considerations, structure-direction in the aluminophosphate system may depend also on many additional factors, including the concentration of the SDA,[18,19] and the source of reactants.[20] Here we have investigated the structure direction of 1,2,3-trimethylimidazolium (123TMI) in the synthesis of $AlPO_4$ and SAPO materials. This cation is the organic structure-directing agent (OSDA) most specific for ITW in the pure silica system when F^- is also present.[2]

---

[a] *Center for Ordered Nanoporous Materials Synthesis, School of Environmental Science and Engineering, POSTECH, Pohang 790-784, Korea; E-mail: sbhong@postech.ac.kr*

[b] *Departamento de Química Física, Universidad del País Vasco (UPV/EHU), Apartado 644, 48080, Bilbao, Spain.*

[c] *Instituto de Ciencia de Materiales de Madrid (ICMM), Consejo Superior de Investigaciones Científicas (CSIC), Sor Juana Inés de la Cruz 3, 28039 Madrid, Spain; E-mail: macamblor@icmm.csic.es*

† Electronic Supplementary Information (ESI) available: [TGA/DTA thermal analysis traces, ex-situ variable temperature XRD patterns of PST–27, XRD patterns of triclinic $AlPO_4$–34 before and after calcination at 550 and 1000 °C, FESEM image of $AlPO_4$–34 calcined at 1000 °C, orthorhombic vs. monoclinic indexing of PST–27, extra reflections in PST–27, details of the structure solution of $AlPO_4$–34 (including Rietveld plot, crystallographic and experimental parameters, fractional coordinates, and views of the occluded dimer), UV-vis spectra, emission and excitation spectra for all samples, characterization (XRD, TGA/DTA, chemical composition) of SAPO–34 phases.]. CCDC 1455308. See DOI: 10.1039/b000000x/

Three different phases have been obtained, depending on the content of OSDA and/or water in the $AlPO_4$ synthesis mixtures: HPM–3, PST–27, and a triclinic $AlPO_4$–34 (CHA). HPM–3, containing a high organic content (ca. 26 wt%), is still under investigation and will be reported elsewhere. PST–27 is a monoclinic version of $AlPO_4$–5 (AFI). Each *cha*-cage in as-made triclinic $AlPO_4$–34 contains a cationic dimer with a short distance (< 3.8 Å) between the center of the aromatic rings, possibly pointing to a role of self–aggregation through $\pi - \pi$ interactions in the crystallization of this particular material. As found in another triclinic $AlPO_4$–34 material reported by Oliver and coworkers,[21] the material shows a high thermal stability, withstanding calcination up to at least 1000 °C. In addition, there are different calcined phases depending on the level of hydration.[22]

2 Experimental

2.1 Synthesis

A concentrated aqueous solution of 1,2,3-trimethylimidazolium hydroxide (123TMIOH) was prepared as previously reported.[2] In a typical procedure for the crystallization of the $AlPO_4$–based microporous solids, an aluminophosphate gel was prepared by combining aluminum hydroxide $Al(OH)_3$, (Aldrich, 85.3 wt% determined by thermogravimetry) with 123TMIOH followed by drop-wise addition of *o*–H_3PO_4 (85%, Aldrich). The mixture was stirred and then HF (48%, J.T. Baker) was added and stirring was maintained for 25 min at room temperature. When necessary, a small amount of tetraethylorthosilicate (TEOS, 98%, Aldrich) was added. In addition, if required, the resulting gels were condensed by evaporation, and the amount of water evaporated was monitored by weight. The final gel composition was x 123TMIOH : 1 Al_2O_3 : 1 P_2O_5 : 0.4y SiO_2 : z HF : w H_2O, where x is 1.6 or 2.0, y is 0 or 1, z is 1 or 2 and w is 10 or 40. The crystallization was carried out at 150 °C in Teflon-lined 23-mL autoclaves with rotation (60 rpm) under autogenous pressure for 4-7 days. The solid products were recovered by filtration or centrifugation, washed repeatedly with distilled water, and dried overnight.

2.2 Characterization

Phase identification was done by powder X- ray diffraction (XRD). Data were obtained in the 3 – 50° 2θ range on a PANalytical X'Pert diffractometer with Cu K_α radiation and an X'Celerator detector, using a fixed divergence slit (0.50°) and Soller slits (incident and diffracted = 0.04 rad). In situ high-temperature XRD experiments were performed in Bragg-Brentano geometry using the same diffractometer equipped with an Edmund Bühler HDK 1.4 high-temperature attachment. In addition, when necessary, the powder XRD measurements were carried out after calcining the sample in air at variable temperatures up to 800 °C for 4 h. Synchrotron powder XRD data for as-made PST–27 were collected on the 9B beamline equipped with a ceramic furnace of the Pohang Acceleration Laboratory (PAL; Pohang, Korea) using monochromated X-rays (λ = 1.4865 Å). Details of the experimental set up have been described elsewhere.[10] Synchrotron data for as-made triclinic $AlPO_4$–34 were recorded in capillary mode (outer diameter: 0.8 mm) on the BM25A Spanish beam line at ESRF using monochromated X-rays (λ= 0.82548 Å) over the 2θ range 2 – 62°.

Elemental analysis for Al, P, and Si was performed by a Jarrell Ash Polyscan 61E inductively coupled plasma spectrometer in combination with a Perkin-Elmer 5000 atomic absorption spectrophotometer. The C, H, and N contents of the samples were analyzed by using a Vario EL III elemental organic analyzer. Thermogravimetric analysis (TGA) was performed on an SII EXSTAR 6000 thermal analyzer under air flow with ramping rate of 10 °C min^{-1}, and the weight losses related to the combustion of the OSDA were further confirmed by differential thermal analysis (DTA) using the same analyzer. Crystal morphology and size were examined with a FEI NOVA NANOSEM 230 scanning electron microscope (SEM) or a JEOL JSM-6510 SEM.

^1H and ^{13}C solution NMR measurement for OSDA were carried out in 5 mm quartz tubes using a Bruker AVANCE III 300 spectrometer. The ^1H NMR spectra were recorded at a ^1H frequency of 300.13 MHz with a $\pi/2$ rad pulse length of 11.0 μs and a recycle delay of 2.0 s. The ^{13}C NMR spectra were recorded at a ^{13}C frequency of 75.475 MHz with a $\pi/2$ rad pulse length of 10.2 μs and a recycle delay of 1.5 s.

Multinuclear MAS NMR measurements were performed on a Bruker DRX500 spectrometer at a spinning rate of 22.0 kHz. ^1H MAS NMR spectra were recorded at a 1H frequency of 500.130 MHz with a $\pi/2$ rad pulse length 2.5 μs, a recycle delay of 3.0 s and an acquisition of ca. 1000 pulse transients. ^1H–^{13}C CP MAS NMR spectra were measured at a ^{13}C frequency of 125.758 MHz with a $\pi/2$ rad pulse length 4.8 μs and an acquisition of ca. 500 pulse transients, which was repeated with a contact time of 2.0 ms and a recycle delay of 3.0 s. The ^1H and ^{13}C chemical shifts are reported relative to TMS. The ^{27}Al MAS NMR spectra were recorded at a ^{27}Al frequency of 130.318 MHz with a $\pi/6$ rad pulse length 1.0 μs, a recycle delay of 2.0 s and an acquisition of ca. 1000 pulse transients. The ^{27}Al chemical shifts are referenced to an $Al(H_2O)_6{}^{3+}$ solution. The ^{31}P MAS NMR spectra were obtained with a ^{31}P frequency of 202.493 MHz with a $\pi/6$ rad pulse length of 1.7 μs, a recycle delay of 20.0 s and an acquisition of 128 pulse transients. The ^{31}P chemical shifts are reported relative to a H_3PO_4 solution. The ^{19}F MAS NMR spectra were collected using a Varian Unity Inova 600 NMR spectrometer at a ^{19}F frequency of 564.5 MHz and a spinning rate of 25 kHz, with $\pi/2$ rad pulse length of 1.7 μs and a recycle delay of 10 s, and an acquisition of ca. 80 pulse transients. For the quantitative analysis, the weight of each sample was measured and ITQ-12 with a known fluoride content was used as external standard reference.

Diffuse reflectance UV–visible absorption spectra (DRUVS) were recorded using a Shimadzu UV-2600 spectrophotometer with an integrating sphere attachment and $BaSO_4$ was used as the reference. Fluorescence spectra were recorded on a RF-5301 Shimadzu spectrofluorimeter in the front-face (reflection) configuration. Supported sample films, prepared by solvent evaporation of solids suspended in CH_2Cl_2, were oriented 35 ° and 55° with respect to the excitation beam and the detector, respectively. Because of the poor emission capacity of the samples, large slit widths and/or high sensitivity mode were applied.

Table 1 Syntheses from gel composition x 123TMIOH : 1.0 Al_2O_3 : 1.0 P_2O_5 : 0.4y SiO_2 : z HF : w H_2O[a]

Gel Composition				
x	y	z	w	Product[b]
1.6	0	2	10	$AlPO_4$–HPM–3
1.6	1	2	10	SAPO–HPM–3
1.6	0	2	40	$AlPO_4$–PST–27
1.6	1	2	40	PST–27 + triclinic SAPO–34
2.0	0	2	10	$AlPO_4$–HPM–3
2.0	1	2	10	Rhombohedral SAPO–34 (1)
2.0	0	2	40	Triclinic $AlPO_4$–34
2.0	1	2	40	Triclinic SAPO–34
2.0	1	1	40	Rhombohedral SAPO–34 (2)

[a] All syntheses were carried out under rotation (60rpm) at 150 °C [b] The product appearing first is the major phase.

3 Results and discussion

3.1 Synthesis and physicochemical characterization

Table 1 lists the representative products obtained from a series of syntheses using 123TMIOH as an OSDA and $AlPO_4$ or SAPO gels with different compositions under the conditions described above. These data reveal that three different phases can be obtained from the Si-free $AlPO_4$ system, all with a high crystallinity, depending on the OSDA and/or water contents: HPM–3, PST–27 and triclinic $AlPO_4$–34. It is also remarkable that these three materials are stable under the crystallization conditions for one additional week. HPM–3, which was obtained at the most concentrated conditions, is still under study and will be reported after further advancing on its characterization. When a small amount of Si (Si/P = 0.2) is added to the $AlPO_4$ gel, on the other hand, we were able to obtain HPM–3 but not PST–27 in pure form. Also, rhombohedral SAPO–34 was the phase crystallized from a SAPO gel with a higher 123TMIOH/Al_2O_3 ratio (2.0) but either with half HF content (entry 9) or a lower H_2O/Al_2O_3 ratio (10) (entry 6 in Table 1). However, an increase in H_2O/Al_2O_3 ratio to 40 gave SAPO–34 with triclinic instead of rhombohedral symmetry (entry 8).

Chemical composition data of as-made PST–27 and triclinic $AlPO_4$–34 are collected in Table 2. The Al/P ratio is close to 1 in both phases. The C/N ratio is always close to the value in the pristine 123TMI (3.0), and this is also the case for the H/N ratio (5.5 in 123TMI) in triclinic $AlPO_4$–34. However, there is a very large excess of hydrogen in as-made PST–27, that may be assigned to ca. 8.3% water, which neatly corresponds to the first step in the TG trace (8.7 wt%; see Supporting Information Figure S1, left). The second step, which is exothermic in nature, would presumably be due to the decomposition/combustion of 123TMI$^+$F$^-$ and amounts to 11.46% (compared to a 123TMIF content of 11.45 % based on N analysis). The fluoride content, determined by quantitative ^{19}F MAS NMR (see Experimental section) supports the charge of organic cations is fully balanced by fluoride in triclinic $AlPO_4$–34. However, there is an apparent excess of fluoride over cations in PST–27.

PST–27 transforms into $AlPO_4$–5 upon calcination (Figure 1). Ex situ variable–temperature powder XRD experiments on this phase reveal that the transformation occurs above 300 ° C and is essentially completed at 400 ° C (Supporting Information Figure S2). Depending on the calcination conditions, some tridymite-like dense $AlPO_4$ may also be formed at temperatures higher than 600 ° C, and this is the dominant phase when the calcination temperature is much higher.

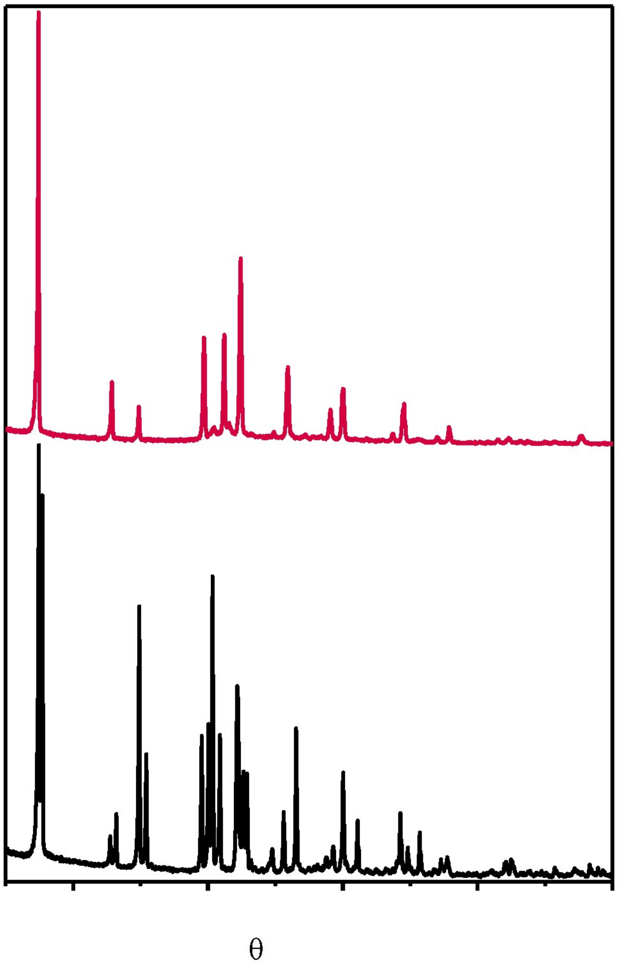

Fig. 1 Powder XRD patterns of as-made (bottom) and calcined PST–27 (top). The asterisks mark reflections from a tridymite-like $AlPO_4$ impurity formed upon calcination.

As-made PST–27 crystallizes as relatively large (ca. 30μm wide and 60 μm large) distorted hexagonal prisms (Figure 2).

On its turn, triclinic $AlPO_4$–34 crystallizes after heating an $AlPO_4$ gel with 123TMIOH/Al_2O_3 = 2.0 at 150 °C for 4 days. The solid obtained was highly crystalline and its pattern was indexed as triclinic with a = 9.38 , b = 9.29, c = 9.23 Å $\alpha = 90.68, \beta = 102.68, \gamma = 85.19°$ (see Figure S3). Thermogravimetric analysis shows that there is a very large weight loss occurring essentially in a single step around 500-530 °C (ca. 26.7 wt%), with only a minor weight loss of 0.6 wt% in the 200-400 °C range (Figure S1, right). The solid residue after TGA/DTA up to 1000 °C was found to be still crystalline showing its outstanding stability, and the large difference in powder XRD pattern from the calcined form of triclinic $AlPO_4$–34 is attributed to different degrees of rehydration (compare Supporting Information Figure

Table 2 Elemental Analysis of as-made PST–27 and triclinic $AlPO_4$–34

			wt%					molar	ratios	
Phase	Al	P	N	C	H	F	Al/P	C/N	H/N	TMI/F
PST–27	17.21	18.86	2.47	6.48	1.92	2.64	1.05	3.06	10.8	0.63
triclinic $AlPO_4$–34	13.64	16.45	5.58	14.71	2.29	4.13	0.95	3.07	5.7	0.92

S4 with Figure S3, top).[22]

As-made triclinic $AlPO_4$–34 crystallizes as very uniform, asymmetric and thin crystallites (a representative crystal measures roughly $18 \times 7 \times 2 \mu m^3$; Figure 2). After thermal analysis, the morphology is maintained, although the crystals are largely cracked (Figure S5). Elemental analysis of the as-made sample indicates the Al/P and F/N molar ratios are close to 1 and 0.5, respectively, as expected. This, together with the TGA/DTA results, reveals an ideal composition of $[C_6N_2H_{11}]_2[Al_3P_3FO_{12}]_2 : 1/3H_2O$, for the triclinic unit cell described below. Water is included to account for the weight lost at relatively low temperature, although this assignation is dubious because most of that weight is lost above 200 °C (Figure S1, right).

3.2 NMR spectroscopy

Multinuclear MAS NMR spectra of the as–made and calcined forms of PST–27 and triclinic $AlPO_4$–34 are presented in Figures 3, 4, 5, 6.

In the ^1H–^{13}C CP MAS NMR spectrum of PST–27 (Figure 3, top), four sharp resonances at 8.5, 36.4, 123.8 and 143.8 ppm are assigned to the carbon atoms in the methyl substituents at C(2) and at both nitrogen atoms, and to both types of aromatic carbons (C(2) and C(4)=C(5)), respectively, indicating that the OSDA remains intact upon its occlusion. The very broad resonances in the ^1H MAS NMR spectra of triclinic $AlPO_4$–34 (Figure 3, bottom) suggest a largely restricted motion of the organic cation, which may be actually locked in position, while it appears to be more mobile in PST–27. In the ^1H–^{13}C CP MAS NMR spectrum of triclinic $AlPO_4$–34, all the ^{13}C resonances assigned to the imidazolium ring are split, suggesting two different local environments.

The ^{27}Al MAS NMR spectrum of as-made PST–27 (Figure 4) reveals the existence of at least five different Al species, including two octahedral Al environments around -17 and -9 ppm, one penta–coordinated Al around 13 ppm and no less than two tetrahedral Al species around 38 and 43 ppm. Its ^{31}P MAS NMR spectrum (Figure 6) was found to be also complex: at least four different ^{31}P resonances around -27, -23, -20(sh) and -14 ppm with largely dissimilar intensities are observable. The complex nature of PST-27 can also be concluded from its ^{19}F MAS NMR spectrum (Figure 5), because there are at least five environments for fluoride (chemical shifts around -118, -119(sh), -120, -126, and -184 ppm), together with many spinning side bands that forced us to check true resonances at different spinning speeds. In general, the multinuclear MAS NMR spectra of as–made PST–27 reveal that this material is a extremely complex phase, with complex line shapes and many more environments for Al and P atoms than expected for the relatively simple AFI structure with only one topological tetrahedral site (T-site). After calcination, however, its ^{27}Al MAS NMR spectrum became simpler: three resonances appearing at 39.6, 9.4 and -11.5 ppm (Figure 4) can be assigned to tetrahedral, pentacoordinated and octahedral Al species, respectively. As shown in Figure 6, in addition, the ^{31}P MAS NMR spectrum of calcined PST–27 shows a strong but broad and asymmetric resonance at -28 ppm.

On the other hand, the ^{27}Al MAS NMR spectrum of as-made triclinic $AlPO_4$–34 shows an intense and asymmetric resonance at 38.2 ppm due to tetrahedral Al and a smaller and much broader resonance at -20.9 ppm, assignable to octahedral Al, in agreement with the structural characterization (see below). After calcination and rehydration, however, three resonances at 39.9, 14.8 and -13.6 ppm, which are assigned to tetrahedral, penta–coordinated and octahedral Al species, respectively, are observed. This strongly suggests coordination of water to framework Al, in accord with a previous report on triclinic $AlPO_4$–34.[22]

The ^{31}P MAS NMR spectrum of as-made triclinic $AlPO_4$–34 is characterized by three resonances with about equal intensities at -9.2, -25.2 and -30.2 ppm. Again, the existence of three different environments for tetrahedral P atoms (Figure 6) agrees with the structural characterization (see below). The spectrum is similar to that of as-made UT-6, the piperidinium fluoroaluminophosphate chabazite precursor reported by Oliver et al. (resonances at -8.5, -25.2 and -31.1 ppm).[21] After calcination and rehydration, a prominent resonance at -27 ppm evidences more uniform environments for P, although a shoulder around -22 ppm may be due to the framework distortion caused by coordination of water to some framework Al atoms.

The ^{19}F MAS NMR spectrum of triclinic $AlPO_4$–34 (Figure 5) shows a main resonance at -121.3 ppm and a much smaller one at -126.9 ppm. The very weak intensity of the latter suggests it may come from an impurity in this particular sample used for the NMR measurement. We note here that the former resonance appears at a similar chemical shift as in UT-6 (-120 ppm), in which fluoride also bridges two framework Al atoms across what would become a 4MR after calcination.[21] We also note that none of the phases obtained in this work, including HPM–3 (spectrum not shown), contains fluoride occluded within D4R units, which would be characterized by a ^{19}F MAS NMR resonance in the chemical shift range between -65 and -95 ppm.[23]

3.3 Structural Characterization

3.3.1 PST–27.

The low–resolution powder XRD pattern of as-made PST–27 recorded with Cu K_α radiation was indexed as orthorhombic (a=13.91Å, b=22.99Å, c=8.51Å). Although this indexing is compatible with the structure of calcined $AlPO_4$-5 reported by Mora

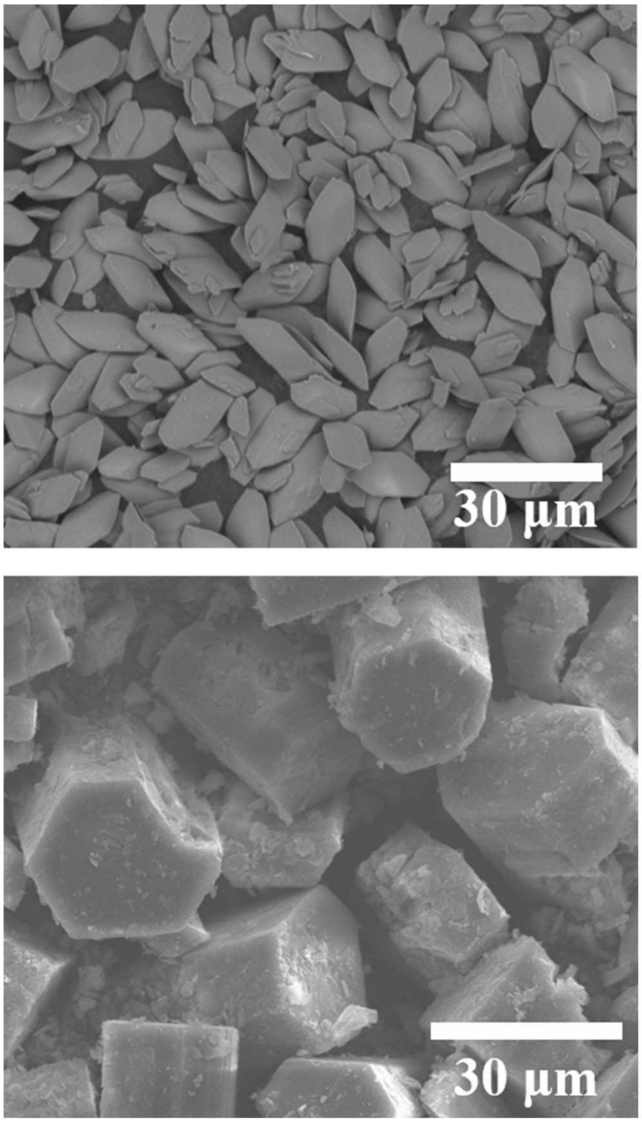

Fig. 2 FE-SEM images of as-made PST–27 (bottom) and triclinic AlPO$_4$–34 (top).

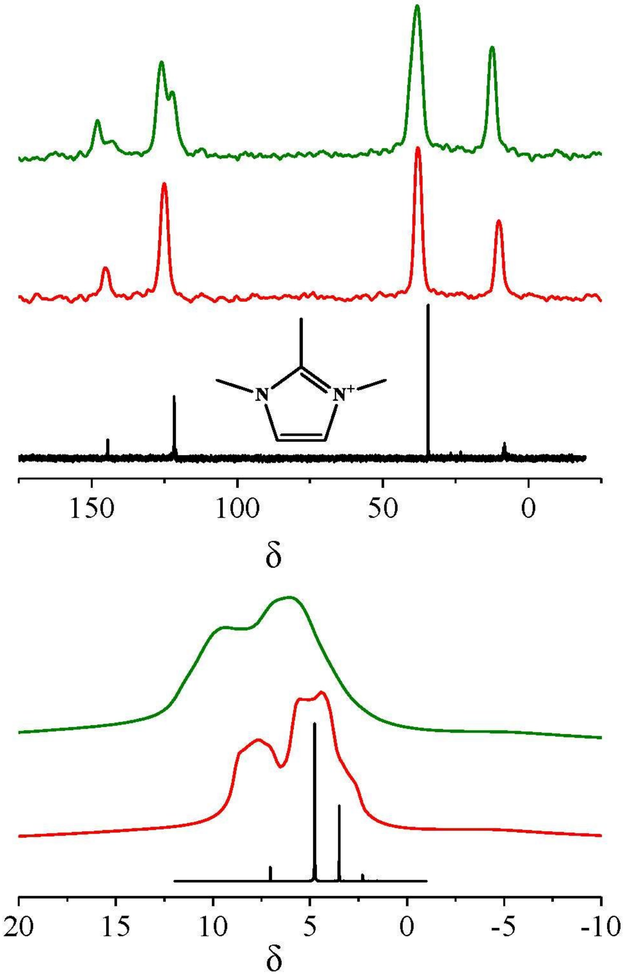

Fig. 3 ^{1}H (bottom) and ^{1}H–^{13}C CP (top) MAS NMR spectra of as-made triclinic AlPO$_4$–34 (green) and PST–27 (red). The black trace is the ^{1}H (bottom) or ^{13}C (top) NMR of 123TMI iodide in D$_2$O solution.

(a = 13.794, b = 23.900, c = 8.4168 Å, space group *Pcc*2),[24], the orthorhombic distortion with respect to the hexagonal AFI structure is much larger in PST–27. The degree of orthorhombic distortion can be quantified as the deviation of $(a * \sqrt{3})/b$ from 1. This gives exactly 1.00 for Mora's calcined AlPO$_4$-5, while in our case, using an orthorhombic indexing of the synchrotron data (a= 13.9198, b=23.009, c=8.512Å) it gives 1.05 for as-made PST–27. Moreover, the synchrotron powder XRD data of PST–27 revealed the splitting of some intense peaks (see Figure S6), while many very weak reflections that were unclear in the first pattern showed up (Figure S7). The additional reflections could not be indexed (see below), but the splitting could be accounted for by a small monoclinic distortion (0.2°), with final cell parameters of a=13.9201, b=23.010, c=8.512 Å β=90.207 ° in space group *Pc*. While the AFI Zeolite Framework Type contains only one topologically distinct T–site with a multiplicity of 24, our double monoclinic cell should have 24 sites (12 Al, 12 P), all with a multiplicity of 2. However, this more complex structure cannot explain the large complexity observed in the ^{27}Al and ^{31}P MAS NMR spectra of as-made PST–27 (Figures 4 and 6, respectively). For instance, the ^{31}P resonances at lower field has a total apparent intensity (without considering spinning side bands) of ca. one tenth of the total intensity of the two resonances (plus a shoulder) at higher field.

On the other hand, the origin of the extra reflections commented above is still unclear. They apparently do not belong to an impurity phase, because all PST–27 samples, which were obtained from eight different batches after 4 or 7 days of crystallization at 150 °C, show such reflections with quite similar relative intensities. Thus, these reflections may likely belong to PST–27, and might be due to either a farther distortion of the structure, or to a supercell or to an incommensurate modulation, as the one observed in SSZ-24, the pure-silica version of the same AFI topology.[25] We have not been able to find an adequate indexing of the extra reflections, even by an extensive search using dicvol,[26] allowing for much larger and less symmetric triclinic cells. Thus, while PST–27 is clearly a precursor to AlPO$_4$-5, its nature appears to be rather complex, as evidenced by its powder XRD and ^{27}Al and ^{31}P MAS NMR data.

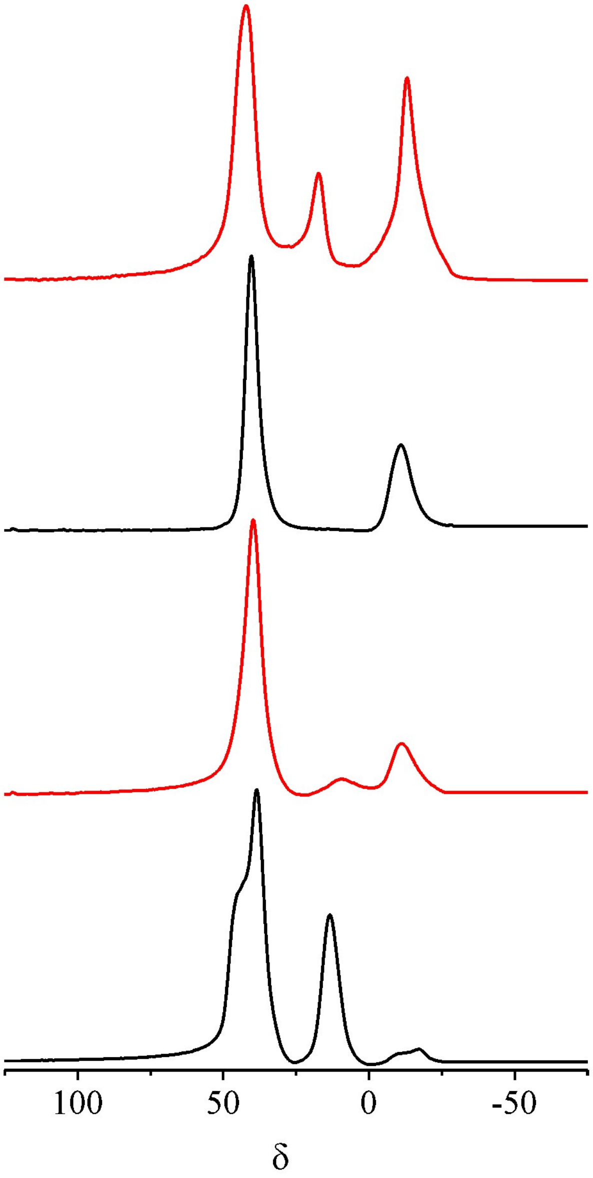

Fig. 4 ^{27}Al MAS NMR spectra of as-made (a) and calcined (b) PST–27 and as–made (c) and calcined (d) $AlPO_4$–34.

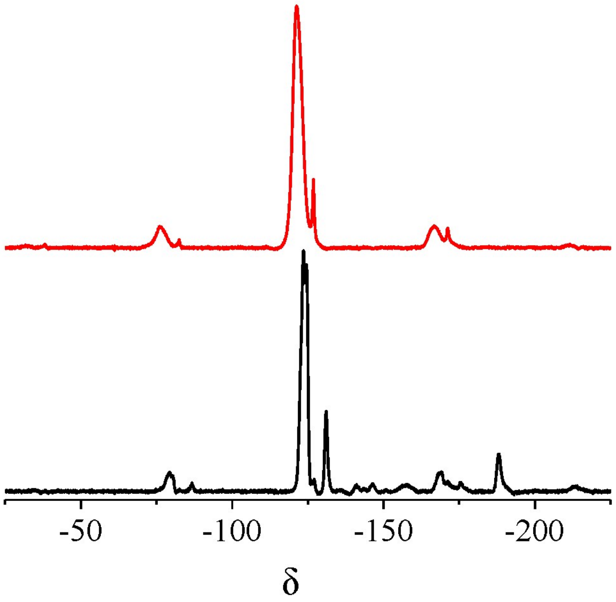

Fig. 5 ^{19}F MAS NMR spectra (at a spinning rate of 25 kHz) of as-made PST–27 (bottom) and $AlPO_4$–34 (top). Spinning side bands are marked with *.

3.3.2 Triclinic $AlPO_4$–34.

A model for triclinic $AlPO_4$–34 obtained by direct methods (see Supporting Information) in space group $P\bar{1}$ and initially with only Al, P, O and F, was used as a starting model in the Rietveld refinement using the GSAS suite of programs,[27] and the EXPGUI graphical interface.[28] The model contained three crystallographic positions for tetrahedral P, as well as 2 crystallographic positions for tetrahedral Al and another one for octahedral Al, as fluoride was found to link two Al at the diagonal of a 4MR (see below). Later on, the cation was introduced as a rigid body. Details of the Rietveld analysis are provided as supporting information, with the crystallographic data summarized in Tables S1 and S2 and the final Rietveld plot given in Figure S9. The crystallographic data were deposited with the Cambridge Crystallographic Data Center as supplementary publication CCDC 1455308.

The refined unit cell volume (781.28 Å^3) of our triclinic $AlPO_4$–34 is over 2% larger than the value of any of the previously reported $AlPO_4$–34 materials containing two organic cations and fluoride per *cha*–cage, such as piperidinium UT-6 (759.25 Å^3),[21] and morpholinium fluoroaluminumphosphate (764.7 Å^3),[29] as shown in Table 3, possibly due to the significantly larger size of 123TMI. It is also larger than the volume of cyclam fluoroaluminumphosphate CHA (769.48Å^3), which contains only one doubly charged cation per cavity.[30]

The geometry around the octahedral Al is shown in Figure 7. Equatorial distances are generally shorter (Al-O_{eq} 1.809 $\pm$ 0.020 Al-F 1.876 $\pm$ 0.034) than apical ones (Al-O_{ap} 1.878 $\pm$ 0.025), and the octahedron is slightly distorted. Tetrahedral P-O and Al-O distances are well within the expected values for this class of materials (P-O 1.541 $\pm$ 0.051, Al-O_{tet} 1.734 $\pm$ 0.057).

The location of the aromatic cations inside the *cha*–cage is de-

Table 3 As-made fluoroaluminophosphate materials with the CHA topology

Cation	Organic per u.c.[a]	a, b, c (Å)	α, β, γ(°)	Vol. (Å^3/uc)	d/Å[b]	material
morpholinium$^+$	$2{*}C_4NOH_{10}$	9.162, 9.183, 9.333	86.24, 77.43, 88.45[c]	764.7	4.24	CHA[29]
pyridinium$^+$	$2{*}C_5NH_6$	9.118, 9.161, 9.335	85.98, 77.45, 89.01	759.25	–[d]	UT–6[21]
cyclamH_2^{2+}	$C_{10}N_4H_{26}$	9.099, 9.223, 9.393	77.88, 87.20, 87.78	769.48	–[e]	CHA[30]
13DMI$^+$	$2{*}C_5N_2H_9$	9.074, 9.230, 9.309	76.45, 87.34, 89.39	757.13	3.79	SIZ–10[31]
1E3MI$^+$	$2{*}C_6N_2H_{11}$	9.090, 9.207, 9.291	76.55, 87.30, 89.41	755.45	3.75	SIZ–4[32]
123TMI$^+$	$2{*}C_6N_2H_{11}$	9.228, 9.286, 9.379	85.21, 77.31, 89.35	781.28	3.78	$AlPO_4$–34[h]

[a] All crystallize in space group $P\bar{1}$, and the corresponding composition of the fluoroaluminophosphate framework is $Al_6P_6O_{24}F_2$. [b] distance between the geometric center of both rings of the dimer inside a *cha*–cage. [c] the conventional cell reported[29] has been reduced. [d] unreported structure, 3.93 Å in the isomorphous $GaPO_4$–UT–6.[33] [e] monomer. [f] 1,3–dimethylimidazolium. [g] 1–ethyl–3–methylimidazolium. [h] This work.

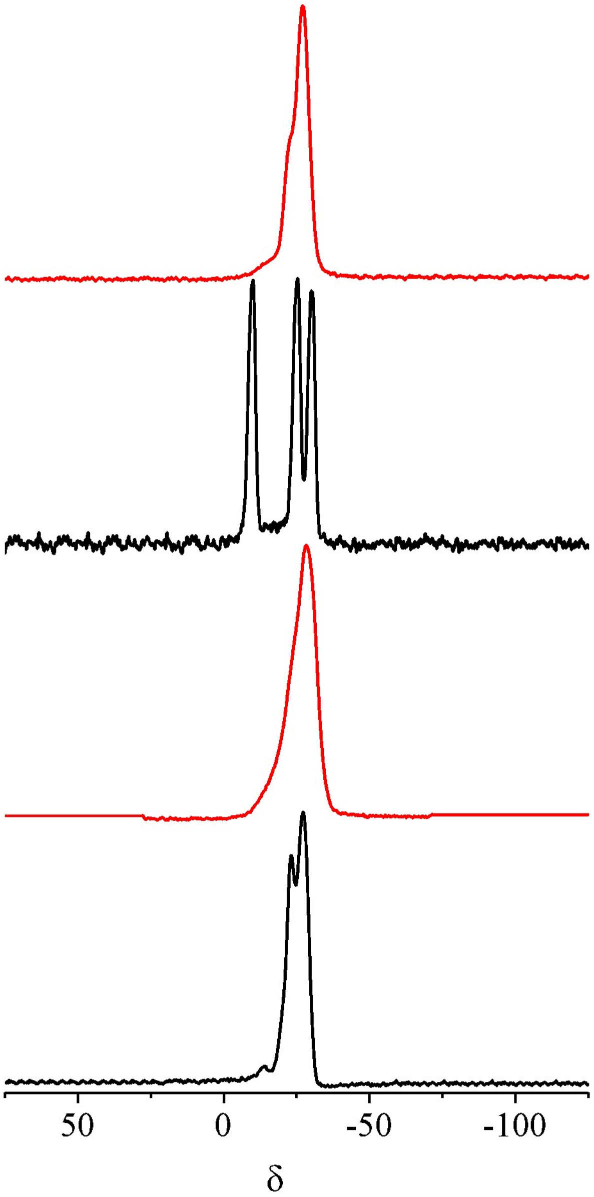

Fig. 6 ^{31}P MAS NMR spectra of as–made (a) and calcined (b) PST–27 and as-made (c) and calcined (d) $AlPO_4$–34.

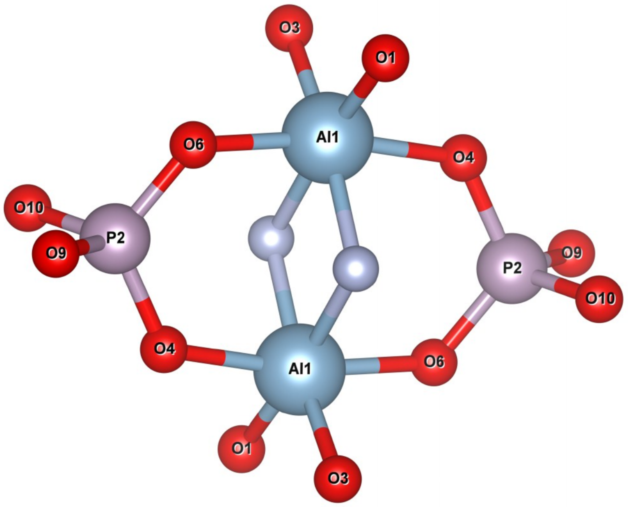

Fig. 7 A structural unit that contains the slightly distorted octahedral Al of the as-made triclinic $AlPO_4$ structure. This unit transforms into a 4MR upon calcination and removal of fluoride.

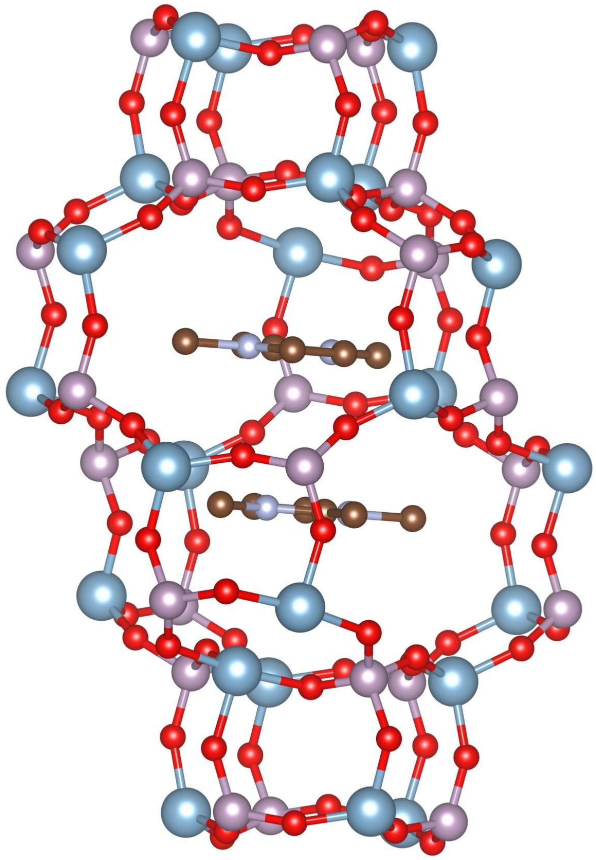

Fig. 8 The location of two 123TMI cations inside the *cha*–cage in as–made triclinic AlPO$_4$–34. Atom colors as in Figure 7 plus bronze (C) and grey (N).

picted in Figure 8. Despite charge repulsion, the distance between both cations is relatively short (3.78 Å), when measured between the geometric centers of both rings (the parallel planes defined by the rings are a bit closer, 3.63 Å). Hence, the conformation may be described as a $\pi-\pi$ stacked parallel displaced dimer with antiparallel dipoles (see also Figure S10). This raises the question of a possible role of self-aggregation through $\pi-\pi$ interactions in the structure-direction of 123TMI towards the CHA structure, although the fact that non-aromatic dimers have also been found in other AlPO$_4$–CHA materials (see Table 3) may somehow detract from this hypothesis. The ring-to-ring distance between dimers found inside other AlPO$_4$–34 phases has been calculated from the reported structures and listed in Table 3. In the case of morpholinium AlPO$_4$–CHA the distance is 4.24 Å. In the case of pyridinium UT-6, the original report did not provide the detailed crystal structure, but in the isomorphous GaPO$_4$ material the ring-to-ring distance is 3.93 Å, which may also point to $\pi-\pi$ interactions. The smallest distance between the center of rings in adjacent cavities in 123TMIF–AlPO$_4$–34 is much longer (6.95 Å).

3.4 UV–vis absorption and emission spectroscopies

In an attempt to characterize the $\pi-\pi$ interactions in triclinic 123TMIF–AlPO$_4$–34, we have studied the UV–vis absorption (Figures 9 and 10) and fluorescence properties (Figures 11 and 12) of

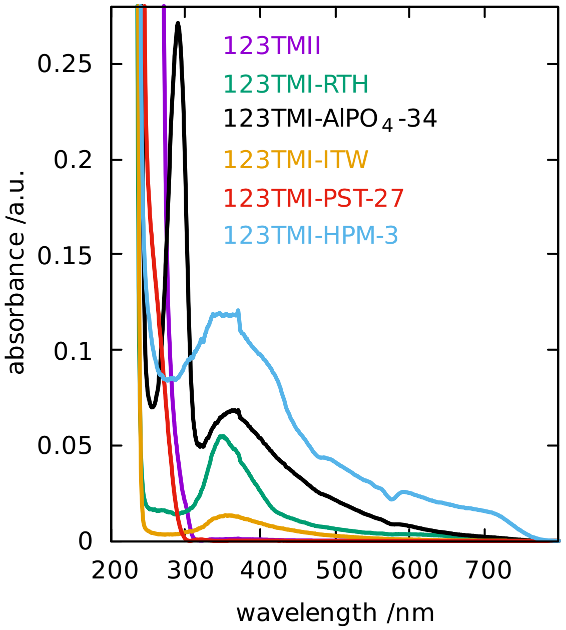

Fig. 9 UV–vis spectra of several solids containing 123TMI.

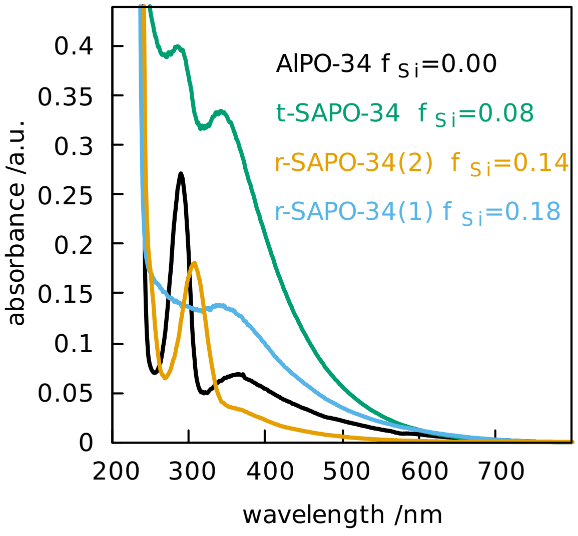

Fig. 10 UV–vis spectra of AlPO$_4$–34 and SAPO–34 materials with different Si contents (molar fraction indicated).

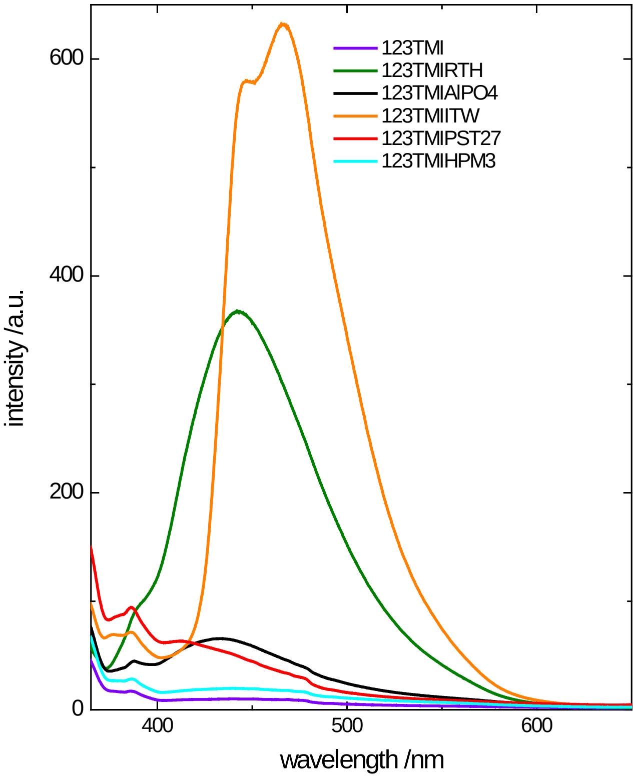

Fig. 11 Emission spectra (excitation at 350 nm) of several solids containing 123TMI (excitation and emission slits 10 and 3 nm, respectively).

a series of materials containing the same cation: 123TMI iodide, pure–silica 123TMI-ITW (where cations are confined in silica cavities and isolated from each other),[2] aluminosilicate 123TMI-RTH (where the cations form a displaced dimer inside a zeolite cavity),[10] and 123TMI-PST–27 and HPM–3(where the cation is in an unknown aggregation state). The iodide salt shows two absorption bands with similar intensities at 216 and 249 nm (Figure S11), while the spectra of all the zeolite-like materials are dominated by one strong band in the 210–220 nm region, with only a very weak and broad band at higher wavelengths (340–370 nm). Only triclinic $AlPO_4$–34 presents a clear additional band at 291 nm that could be due to a transition specific of the $\pi - \pi$ dimer.

Interestingly, introduction of Si into the $AlPO_4$–34 framework led to notable changes in the UV–vis spectrum (Figure 10). This suggests that the interactions between the organic dimer and the inorganic framework largely modifies the optical properties of the cation. The powder XRD patterns (Figure S12), TGA/DTA analysis (Figure S13) and chemical composition (Table S3) data of the three SAPO–34 phases with different Si contents are supplied as Supplementary Information and show that the materials are highly crystalline and always contain two cations per cage. As Si is introduced in the framework, the absorbance band at 291nm slightly change its position, significantly decreases in intensity and even completely vanishes for r-SAPO–34(1) with the highest Si content (Figure 10). It is at present unclear whether this is due to changes in the dimer arrangement (such as a larger displacement or a rotation of one cation with regard to the other).

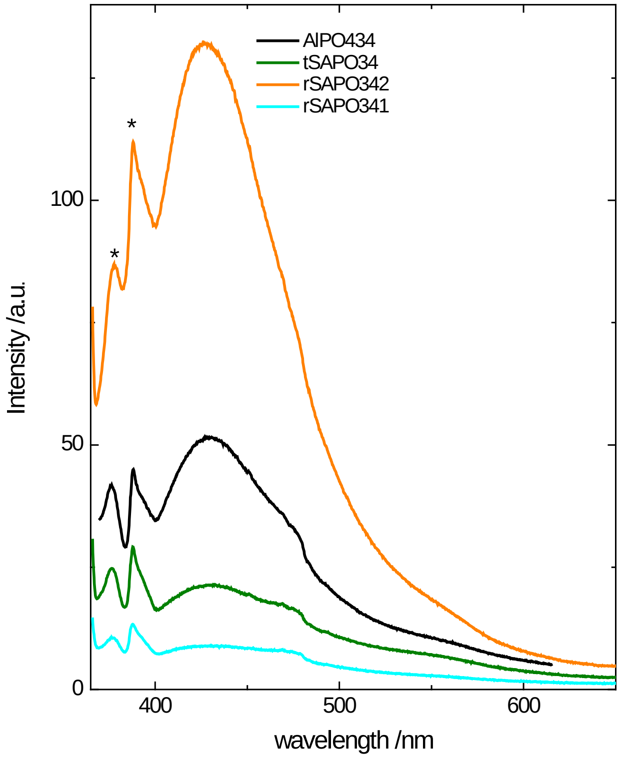

Fig. 12 Emission spectra (excitation at 350 nm) of $AlPO_4$–34 and SAPO–34 materials with different Si contents (high sensibility, excitation and emission slits 3 and 1.5 nm, respectively). Sharp peaks at short wavelengths (denoted as *) are assigned to Raman signals since they shift with the excitation wavelength.

The emission ability of the materials was found to be still more complex. There are few reports on the fluorescence properties of imidazolium cations, which had generally been considered as transparent in most of the UV region and all the visible region and have been used as solvents for studying the optical properties of other molecules.[34] The reported studies thus usually refer to imidazolium cations in very highly concentrated states. Several studies have concluded that pure imidazolium salt do absorb and typically show an interesting fluorescence that depends on the excitation wavelength.[35] This excitation wavelength dependent fluorescence may also occur in solutes dissolved in ionic liquids.[36]

In the case of our imidazolium cation, a weak and unstructured emission band centered at 431 nm is observed for a concentrated 1.0 M solution of 123TMI iodide in water after excitation at 350 nm (Figure S14). This fluorescence band practically vanishes by diluting the sample or under excitation at 220 nm. The steady-state fluorescence spectra of the solid samples containing 123TMI under excitation at 350 nm are shown in Figure 11. Pure 123TMI does not present clear emission bands, but it can emit when included in the microporous materials presented here. 123TMI-ITW presents a structured fluorescence band with two overlapping peaks at 447 and 465 nm, which are independent of the excitation wavelength in the 350–400 nm range (which is the only excitation band detected in the UV, Figure S15). This band can be assigned to the emission of 123TMI monomers isolated in the ITW silica cage. The CHA–type 123TMI–AlPO$_4$–34 presents an unstructured and weak fluorescence band centered at 434 nm. According to the exciton theory, a perfect sandwich dimer does not fluoresce, while the emission from a distorted (twisted or displaced) sandwich dimer should be very weak and placed at higher wavelengths with respect to the emission from the monomer. Indeed, 123TMI–AlPO$_4$–34 presents two weak excitation bands centered at 260 and 355 nm (Figure S15). Excitation at 250 nm leads to two emission bands at 360 and 434 nm, and the intensity of the former band progressively decreases with increasing the excitation wavelength up to 380 nm (Figure S16). The fluorescence of 123TMI–RTH is between those of 123TMI–ITW and 123TMI–AlPO$_4$–34: a wide and moderate emission band at 432 nm, with two excitation bands at 282 and 375 nm and a slight shift in the emission band with the excitation wavelength in the 230-390 nm range. Finally, 123TMI–PST–27 and 123TMI–HPM–3 do not present any clear fluorescence band.

On the other hand, 123TMI–SAPO–34 materials present a similar fluorescence band to that of 123TMI–AlPO$_4$–34 (Figure 12), although its intensity depends on the Si content, being most intense for the rhombohedral sample 123TMI–r–SAPO–34(2) with a Si molar fraction of 0.14 (1.7 Si atoms per unit cell). In this last case, the emission shows an important dependence on the excitation wavelength (Figure S17). In fact, excitation of 123TMI–r–SAPO–34(2) in the 240-390 nm range leads to two emission bands centered around 365 and 425 nm (Figure S17). The former band decreases in intensity when increasing the excitation wavelength, so that it practically disappears when exciting at 310 nm or longer. On the other hand, the emission band at 425 nm progressively shifts to longer wavelengths when the excitation wavelength increases from 340 to 390 nm. This so-called "red-edge effect" (REE), i.e., the red shift of the maximum of the fluorescence band when the excitation wavelength is shifted towards the red–edgee of the absorption band, was discovered in the 1970's and is attributed to the existence of a distribution of energies in the excited state due to different interactions of the fluorophores (the solute molecules) with the environment (the solvent molecules encaging the solute), coupled with a slow relaxation of that environment.[37] On this light, we may consider unexpected that the REE manifests in the case of the triclinic AlPO$_4$–34 material, in which the "solute" is in a well–defined state inside a well defined "solvent cage" (the inorganic framework).

4 Conclusions

Using 123TMI and fluoride we have synthesized three AlPO$_4$ (HPM–3, PST–27, and triclinic AlPO$_4$–34) and three SAPO (SAPO–HPM–3 and triclinic and rhombohedral SAPO–34) phases. HPM–3 crystallizes only at low water contents, and its structure is so far unknown. PST–27 is a distorted and complex precursor of AlPO$_4$–5, to which it transforms upon calcination. Triclinic AlPO$_4$–34 with the CHA topology has two cations per large cavity, forming a displaced antiparallel dimer, and fluoride bridging two framework octahedral Al. The close distance between the cations suggests $\pi - \pi$ interactions may play a significant role in the crystallization of this phase. The cationic dimer could be responsible for an absorption band at 291 nm, which is completely absent in pure 123TMI iodide, 123TMI–PST–27, 123TMI–SiO$_2$–ITW, and 123TMI–(Al,Si)O$_2$–RTH. This absorption band is largely sensitive to the introduction of Si in the AlPO$_4$–34 framework.

The structure-directing ability of 123TMI in the AlPO$_4$ and SAPO systems in the presence of fluoride is drastically different from that exerted by these two ions in the silica and aluminosilicate systems. This is not unexpected because all the phases obtained in the latter two systems contain 5MR that cannot exist in the AlPO$_4$–based system if Al and P need to alternate. However, it is noticeable that none of the AlPO$_4$ or SAPO phases obtained here contain fluoride occluded in double four ring units. While F$^-$ has been considered to structure-direct towards zeolites with D4R,[11–15] a recent interpretation based on DFT calculations supports that, rather than structure–directing, this anion simply relaxes strained structures (such as D4R-containing silica zeolites) making them attainable by enhancing the flexibility of the framework.[2,6,38] Under this interpretation, the lack of D4R structures in the AlPO$_4$–based structures in this work seems less surprising.

5 Acknowledgements

The authors thank financial support by the Spanish Ministry of Economy and Competitiveness (Project MAT2012-31759) and by the National Creative Research Initiative Program (2012R1A3A2048833) through the National Research Foundation of Korea. Thanks are also due to the BM25 Spline staff at ESRF in Grenoble (France), particularly to G. Castro, and to the staff at PAL in Pohang (Korea). We are also thankful to C. Belver and L. Villaescusa for help in collecting the synchrotron powder XRD data in Grenoble and for helpful discussions.

References

1 H. Pastore, S. Coluccia and L. Marchese, *Annu. Rev. Mater. Res.*, 2005, **35**, 351–395.

2 A. Rojas, E. Martinez-Morales, C. M. Zicovich-Wilson and M. A. Camblor, *J. Am. Chem. Soc.*, 2012, **134**, 2255–2263.

3 A. Rojas and M. A. Camblor, *Angew. Chem., Int. Ed.*, 2012, **51**, 3854–3856.

4 A. Rojas, L. Gomez-Hortigüela and M. A. Camblor, *J. Am. Chem. Soc.*, 2012, **134**, 3845–3856.

5 A. Rojas, L. Gomez-Hortigüela and M. A. Camblor, *Dalton Trans.*, 2013, **42**, 2562–2571.

6 A. Rojas, M. Luisa San-Roman, C. M. Zicovich-Wilson and M. A. Camblor, *Chem. Mater.*, 2013, **25**, 729–738.

7 A. Rojas, O. Arteaga, B. Kahr and M. A. Camblor, *J. Am. Chem. Soc.*, 2013, **135**, 11975–11984.

8 A. Rojas and M. A. Camblor, *Chem. Mater.*, 2014, **26**, 1161–1169.

9 A. Rojas and M. A. Camblor, *Dalton Trans.*, 2014, **43**, 10760–10766.

10 D. Jo, J. B. Lim, T. Ryu, I.-S. Nam, M. A. Camblor and S. B. Hong, *J. Mater. Chem. A*, 2015, **3**, 19322–19329.

11 P. Caullet, J. L. Guth, J. Hazm, J. M. Lamblin and H. Gies, *Eur. J. Sol. State Inor.*, 1991, **28**, 345–361.

12 M. A. Camblor, L. A. Villaescusa and M. J. Díaz-Cabañas, *Top. Catal.*, 1999, **9**, 59–76.

13 L. A. Villaescusa, P. A. Barrett and M. A. Camblor, *Chem. Mater.*, 1998, **10**, 3966–3973.

14 L. A. Villaescusa, P. A. Barrett and M. A. Camblor, *Angew. Chem., Int. Ed.*, 1999, **38**, 1997–2000.

15 P. A. Barrett, T. Boix, M. Puche, D. H. Olson, E. Jordan, H. Koller and M. A. Camblor, *Chem. Commun.*, 2003, 2114–2115.

16 X. Yang, M. A. Camblor, Y. Lee, H. Liu and D. H. Olson, *J. Am. Chem. Soc.*, 2004, **126**, 10403–10409.

17 C. Baerlocher and L. B. McCusker, *Database of Zeolite Structures*, accessed on December 3 2015, `http://www.iza-structure.org/databases/`.

18 X. Tong, J. Xu, X. Li, Y. Li, W. Yan, J. Yu, F. Deng, H. Sun and R. Xu, *Micropor. Mesopor. Mat.*, 2013, **176**, 112–122.

19 X. Tong, J. Xu, C. Wang, W. Yan, J. Yu, F. Deng and R. Xu, *Micropor. Mesopor. Mat.*, 2014, **183**, 108–116.

20 L. Xin, H. Sun, R. Xu and W. Yan, *Scientific Reports*, 2015, **5**, 14940.

21 S. Oliver, A. Kuperman, A. Lough and G. Ozin, *J. Mater. Chem.*, 1997, **7**, 807–812.

22 A. Tuel, S. Caldarelli, A. Meden, L. B. McCusker, C. Baerlocher, A. Ristić, N. Rajić, G. Mali and V. Kaučič, *J. Phys. Chem. B*, 2000, **104**, 5697–5705.

23 P. Caullet, J. L. Paillaud, A. Simon-Masseron, M. Soulard and J. Patarin, *C. R. Chim.*, 2005, **8**, 245–266.

24 A. J. Mora, *J. Mater. Chem.*, 1996, **6**, 1831–1835.

25 Z. Liu, N. Fujita, O. Terasaki, T. Ohsuna, K. Hiraga, M. A. Camblor, M. J. Diaz-Cabanas and A. K. Cheetham, *Chem.–Eur. J.*, 2002, **8**, 4549–4556.

26 A. Boultif and D. Louër, *J. Appl. Crystallogr.*, 2004, **37**, 724–731.

27 A. Larson and R. V. Dreele, *General Structure Analysis System (GSAS)*, Los Alamos National Laboratory Report LAUR 86-748, 2004.

28 B. H. Toby, *J. Appl. Crystallogr.*, 2001, **34**, 210–213.

29 M. Harding and B. Kariuki, *Acta Crystallogr. C*, 1994, **50**, 852–854.

30 P. Wheatley and R. Morris, *J. Solid State Chem.*, 2002, **167**, 267–273.

31 E. R. Parnham and R. E. Morris, *Chem. Mater.*, 2006, **18**, 4882–4887.

32 E. R. Cooper, C. D. Andrews, P. S. Wheatley, P. B. Webb, P. Wormald and R. E. Morris, *Nature*, 2004, **430**, 1012–1016.

33 D. S. Wragg, A. M. Z. Slawin and R. E. Morris, *J. Mater. Chem.*, 2001, **11**, 1850–1857.

34 P. K. Mandal, M. Sarkar and A. Samanta, *J. Phys. Chem. A*, 2004, **108**, 9048–9053.

35 A. Paul, P. K. Mandal and A. Samanta, *J. Phys. Chem. B*, 2005, **109**, 9148–9153.

36 P. K. Mandal, A. Paul and A. Samanta, *J. Photochem. Photobiol. A*, 2006, **182**, 113–120.

37 A. P. Demchenko, *Luminescence*, 2002, **17**, 19–42.

38 M. E. Medina, A. E. Platero-Prats, N. Snejko, A. Rojas, A. Monge, F. Gandara, E. Gutierrez-Puebla and M. A. Camblor, *Adv. Mater.*, 2011, **23**, 5283–5292.